Dynamics of ice layers deposited on MgO(001): Quasielastic neutron scattering experiments and molecular dynamics simulations

Céline Toubin, Sylvain Picaud, Paul N. M. Hoang, Claude Girardet, Benjamin Demirdjian, Daniel Ferry, Jean Suzanne

Dynamics of ice layers deposited on MgO(001): Quasielastic neutron scattering experiments and molecular dynamics simulations

C. Toubin, S. Picaud, P. N. M. Hoang, and C. Girardet[a)]
Laboratoire de Physique Moléculaire—UMR CNRS 6624, Faculté des Sciences, La Bouloie, Université de Franche-Comté, F-25030 Besançon Cedex, France

B. Demirdjian, D. Ferry, and J. Suzanne
CRMC2-CNRS,[b)] Campus de Luminy, Case 913, F-13288 Marseille Cedex 9, France

(Received 20 October 2000; accepted 22 January 2001)

The dynamical behavior of a thin film of ice Ih deposited on MgO(001) surface has been investigated both experimentally and theoretically. Incoherent neutron quasielastic scattering experiments, using uniform MgO powders, show that a quasiliquid water layer of monolayer thickness exists at $T=265$ K. The translational mobility of this layer, with a diffusion coefficient $D_t=1.5\times10^{-5}$ cm^2 s^{-1}, is close to that of liquid water. At $T=270$ K, the thickness of the quasiliquid layer increases to about two layers, showing no appreciable change in the D_t value but an increase of the rotational mobility from 6×10^9 s^{-1} to 1.2×10^{10} s^{-1}. Classical molecular dynamics simulations are performed to determine the translational and orientational order parameters and diffusion coefficients of the supported ice film as a function of temperature within 190 and 270 K, and to compare the results with those obtained for bulk ice. It is shown that the whole supported ice film is much more disordered than bulk ice, with melting temperature around 235 K for the TIP4P potential used, while the melting temperatures of the outermost layer are nearly the same (around 220 K) for the supported film and bulk ice. Comparison of the values of the translational and orientational diffusion coefficients obtained in simulation and experiments displays a good agreement. Although the calculated value of the surface melting temperature is underestimated by 15% with respect to the experimental result, the present study indicates clearly the influence of the support on the melting process.
[DOI: 10.1063/1.1355238]

I. INTRODUCTION

Ice surface melting is an actively discussed topic in chemistry and physics because of the key role it plays in natural phenomena such as thunderstorm electrification, and in environmental sciences dealing with the ice catalyzed production of chlorine on polar stratospheric clouds.[1–3] Although the debate about the melting temperature of ice surface is not new, it is still controversial on both experimental and theoretical points of view. Most experiments including x rays, NMR, ellipsometry, and thermal expansion put the temperature above which the liquid phase exists on ice at around 240 K, but relatively large deviations were observed depending on the probe.[4,5] An impressive number of theoretical papers reporting on structural and dynamical properties connected to the melting process were published using molecular dynamics simulations.[5–13] Similar uncertainties were also obtained regarding the occurrence of a liquid-like phase above bulk ice due to the conjunction of several features. First, the initial structure of perfect hexagonal ice is not unique at finite temperature since the proton disordered phase[14] occur with all proton configurations allowed by ice rules approximately equally probable, whereas the proton ordered structure appears to be the most stable at 0 K. This can influence the surface melting process when T increases, especially in the temperature range 190–273 K under interest. Second, the physical quantities that, in principle, should characterize ice melting do not have the same sensitivity in deciding the starting point and the nature of the phase transition. As an example, translational and orientational order parameters do not behave similarly,[5] and an accurate determination of the intersect point of the liquid and solid phase free energies remains difficult.[12] Third, and not least, among the huge number of potentials used in simulations to describe water–water interactions,[15–17] none of them can account accurately for all the experimental data on liquid water or ice. Fourth, the reduced size of the simulation boxes and the necessary short simulation duration limit a direct comparison with experiments on macroscopic ice samples.

A related phenomenon is the behavior with temperature of an ice film supported on a metal or a dielectric substrate. Indeed, from a fundamental point of view, it is tempting to study the first stages of ice melting or liquid water freezing using very thin films (less than 20 Å), because the corresponding experiments are close to the situation considered in simulation, especially regarding the number of implied water layers. As an example, frost heave on plane wings and windows is a crucial technological process which implies both the support and the adsorbate. In this field of research, the understanding of the melting/freezing mechanism seems, to

[a)]Electronic mail: claude.girardet@univ.fcomte.fr
[b)]Also associated with the Universities of Aix-Marseille II and III.

our knowledge, very incomplete. Most of the available data on the ice structure and dynamics have been realized at low temperature (below 180 K). For instance, scanning tunneling microscopy[18] and helium atom scattering experiments[19] have shown that water molecules are arranged according to an Ih ice-like structure on the Pt(111) surface and on other metal substrates. The layer closer to the metal consists of hexagons with oxygen bound to Pt atoms, while the second layer is hydrogen bonded to the first one, and transition to bulk ice is observed at higher water dose. Tensor low-energy electron diffraction (LEED) analysis of Pt supported ice film at 90 K was interpreted[20] in terms of high amplitude oscillations at the ice surface. This raised the question about the surface mobility of water molecules at higher temperature. Surface and bulk diffusions of water molecules on thin ice multilayers supported by Ru(001) were also studied between 140 and 170 K using laser-induced thermal desorption probe.[21,22] The values of the diffusion coefficients were found to be smaller than the experimental resolution ($\leqslant 10^{-9}\,\mathrm{cm^2\,s^{-1}}$) on the surface and to vary from 2×10^{-16} to $4\times10^{-14}\,\mathrm{cm^2\,s^{-1}}$ inside the bulk when T increases from 150 to 170 K.

Water adsorption experiments on insulating surfaces, using infrared and photoelectron spectroscopies, electron and helium atom scatterings, showed the presence of commensurate water monolayers on BaF_2,[23,24] NaCl,[25,26] and MgO.[27–30] The specificity of MgO(001) face as a substrate for ice was evidenced in previous experimental[27–29] and theoretical[30–32] papers. The water monolayer adsorbed directly on the ionic substrate is flat, commensurate with the (001) face of MgO, and very stable even at 273 K,[33] while the upper layers have a hexagonal bulk-like structure without significant hydrogen bonding with the monolayer. Based on these features, MgO, which is a fundamental component of many minerals, can be used as a model to study the melting of an ice film formed by a reduced number of bilayers upon the rigid monolayer.

In this paper, we present a quasielastic neutron scattering (QENS) study of a water film adsorbed on MgO(001) powder within the temperature range 190–270 K, combined with molecular dynamics (MD) simulations. On one hand, translational and orientational mobilities of the water molecules in the film are determined from the evolution of the quasielastic profile shape with temperature. On the other hand, the translational and orientational order parameters characterizing the film structure and the corresponding diffusion coefficients related to the dynamics of the ice layers are calculated using a semiempirical potential to describe the interaction between water molecules.

Section II is devoted to the presentation of the experiments. After a brief description of the experimental setup and conditions, the QENS spectra are discussed as a function of T and the wave vector $\mathbf{Q}$. In Sec. III, the molecular dynamics simulations characteristics and the physical quantities which can be obtained are described, and the results on the order parameters and diffusion coefficients are presented. The comparison between experimental measurements and calculated structural and dynamical properties of the ice film is done in Sec. IV. In addition, these results are also compared to MD simulations performed on bulk ice.

II. EXPERIMENTS

A. Experimental setup

Experiments have been performed at the Laboratoire Leon Brillouin (LLB) at Saclay (France) on the time-of-flight (TOF) spectrometer G6.2 (Mibemol). The wavelength has been set to 8 Å ($E_0=1.28\,\mathrm{meV}$), allowing a scattering vector range $\mathbf{Q}$ from 0.35 to 1.46 $\mathrm{Å^{-1}}$. The energy resolution of the spectrometer is $\Delta E=39.4\,\mu\mathrm{eV}$. There is neither ice nor MgO Bragg reflection within the experimental Q range. Prior to our experiments on ice, vanadium spectra were measured in order to determine the detector's efficiency and the instrumental resolution. All spectra from ice on MgO(001) are obtained by subtracting the background signal due to the cell+MgO. Typical counting times were 10 h.

The MgO substrate is obtained in our laboratory by burning Mg ribbons in air according to a procedure described elsewhere.[34] The result is a MgO powder made of small cubes featuring very uniform (001) facets as shown in adsorption experiments.[35,36] The neutron cell is a stainless-steel cylinder with a diameter of 2 cm and a height of 8 cm, which has been loaded with about 5 g of MgO powder. The adsorbing MgO surface area has been determined by measuring a methane adsorption isotherm at 77 K. Since methane is known to form a $(\sqrt{2}\times\sqrt{2})\mathrm{R45°}$ commensurate monolayer on MgO(001),[36] it is easy to derive the adsorbing area of the powder from the amount of methane adsorbed at monolayer completion. We found a total adsorption area of 47 $\mathrm{m^2}$.

The water used is normal H_2O from Fluka, called *for organic trace analysis*, which contains less than 3×10^{-6}% of organic impurities. It is further purified by many cycles of condensation at $T\sim170\,\mathrm{K}$, pumping, evaporation, and recondensation. An equivalent 5 bilayers (BL) thick film is formed by using classical volumetry. Since a bilayer of hexagonal Ih ice contains a number of molecules which is very close to one molecule of water per MgO(001) surface site (Mg or O), we can evaluate the number of water molecules necessary to form the 5 BL film from the known MgO adsorbing area. A calibrated volumetric system allows us to introduce the desired amount of water into the neutron cell. The water introduction was done at a MgO temperature of 250 K. The cryostat used is a so-called *orange cryostat* of LLB working with liquid helium and allowing to cool down the neutron cell from ambient temperature to 1.7 K. The temperature regulation system allows a temperature stability better than $5\times10^{-2}\,\mathrm{K}$.

B. Incoherent quasielastic neutron scattering models

Neutrons can exchange momentum and energy with moving molecules. Accordingly, a monochromatic incident beam interacts with condensed matter and is scattered quasielastically. When applied to molecules containing hydrogen atoms, QENS measures the dominant incoherent scattering from them. In this case the spectra are dominated by the Fourier transform of the self-correlation function of the H atoms.

In liquid H_2O, the scattering law $S_{\mathrm{incoh}}(Q,\omega)$ can be written, in the quasielastic region, as the convolution of two contributions[4]

$$S_{\text{incoh}}(Q,\omega)=e^{-2W}(S_t(Q,\omega)\otimes S_r(Q,\omega)). \quad (1)$$

The Debye–Waller factor e^{-2W} ($W=Q^2\langle u^2\rangle/6$) measures the delocalization of the proton due to vibrations, while the factors $S_t(Q,\omega)$ and $S_r(Q,\omega)$ represent the contributions from the translational motions and from the low-frequency rotational motions of the water molecule, respectively. In this model the translational and rotational motions are decoupled, an assumption that has to be made to obtain a numerically tractable analytical model.[37] The translational and rotational components of the scattering law $S_{\text{incoh}}(Q,\omega)$ are responsible for a broadening of the experimental elastic peak.

To reproduce the broadening due to translational motions, we have chosen a Brownian molecular motion model

$$S_t(Q,\omega)=\frac{1}{\pi}\frac{D_tQ^2}{\omega^2+(D_tQ^2)^2}, \quad (2)$$

where $\mathbf{Q}$ is the scattering vector and $\hbar\omega=E-E_0=\Delta E$ is the energy gain or loss of the neutron with respect to the incident energy E_0. In the case of anisotropic atomic displacements, we define $D_t^{\parallel}$ and $D_t^{\perp}$, the parallel and normal components (from a given direction $\mathbf{\Delta}$) of the translational diffusion coefficient. The scattering function depends also on the angle χ between $\mathbf{\Delta}$ and the scattering vector $\mathbf{Q}$.[38] For a 2*D diffusion*, $D_t^{\parallel}=0$ and $D_t^{\perp}\neq 0$ correspond to displacements that are confined in the P plane normal to $\mathbf{\Delta}$. The scattering function becomes

$$S_t^{2D}(Q,\omega)=\frac{l}{\pi}\frac{D_t^{\perp}Q^2\sin^2\chi}{\omega^2+(D_t^{\perp}Q^2\sin^2\chi)^2}. \quad (3)$$

Moreover, for our MgO sample, we have to calculate the powder average, i.e., an integration of Eq. (3) over the isotropic distribution of crystallite orientations.

The rotational component is assumed to be given by an isotropic rotational diffusion model. In this model the hydrogen atoms undergo free rotations limited by random collisions with nearest-neighbor molecules. The corresponding scattering law is the superimposition of a Dirac function $\delta(\omega)$ centered at $\omega=0$ and a sum of Lorentzian curves, as

$$S_r(Q,\omega)=j_0^2(Q\rho)\,\delta(\omega)+\frac{1}{\pi}\sum_{l=1}^{\infty}(2l+1)j_l^2(Q\rho)\frac{l(l+1)D_r}{[l(l+1)D_r]^2+\omega^2}. \quad (4)$$

$j_l^2(Q_\rho)$ are spherical Bessel functions and $\rho=0.98$ Å (the O–H distance) is the radius of gyration for the water molecule.[39] The rotational properties are characterized by the rotational diffusion coefficient D_r. Because of the spherical symmetry of the rotation, no powder average is required.

Finally, the theoretical scattering function $S_{\text{incoh}}(Q,\omega)$ [Eq. (1)] must be folded in with the triangular-shaped QENS instrumental resolution, before being fitted to the measured spectra.

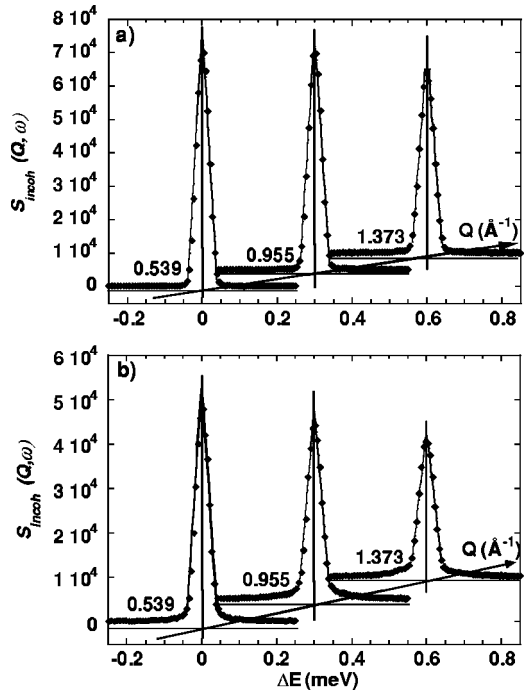

FIG. 1. Evolution of the QENS spectra measured at (a) $T=250$ K and (b) 270 K vs the scattering vector. Experimental spectra are represented by full diamond symbols; the solid lines are the best fit.

C. Fitting procedure and results

We first measure the translational diffusion coefficient D_t at small scattering vector values such that $D_t^{\perp}Q^2\ll D_r$. In these conditions the elastic peak broadening essentially originates from the translational motions since the quasielastic broadening due to rotational motions vanishes at these Q values. It can also be shown that the broadening obeys a D_tQ^2 law.[37] Then, the rotational diffusion coefficient D_r is measured for the higher scattering vector values. The fitting procedure consists of calculating the theoretical scattering function and comparing it with the measured spectra. In the procedure of finding the best agreement between experimental spectra and calculated curves, there are three significant parameters: D_t, D_r, and the proportion of liquid phase in our ice sample. The fit must be correct within all the experimental Q range. The mean-square displacement $\langle u^2\rangle$ in the Debye–Waller factor is taken equal to 0.10 Å^2 under our experimental conditions.

We have measured QENS spectra at four different temperatures: 190, 250, 265, and 270 K. At $T=190$ K there is no measurable broadening of the peaks in the whole Q range, indicating no translation mobility in the 5 BL ice film. Nevertheless, we cannot rule out a translational motion leading to a quasielastic broadening smaller than the instrumental resolution ($D_t\leqslant 10^{-6}$ cm^2 s^{-1}). Therefore, the ice film deposited on MgO(001) is clearly solid at $T=190$ K; the quasielastic broadening observed at higher Q is due to an isotropic rotational motion of the water molecules [Eq. (4)] with a weak rotational diffusion coefficient $D_r=4(\pm 0.5)\times 10^9$ s^{-1}. The situation is the same at $T=250$ K, where no translational mobility is observed in Fig. 1(a), which displays the evolution of the QENS peak profile versus the scattering

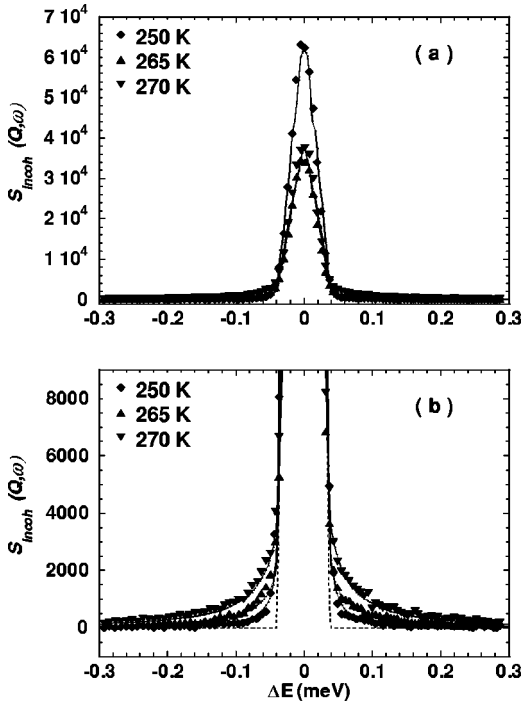

FIG. 2. (a) Evolution of the QENS spectra measured at $Q=1.110\,\text{Å}^{-1}$ vs the temperature. Experimental data are represented by full symbols; the solid lines are the best fit for each temperature. The figure (b) represents a zoom of the figure (a), showing clearly the quasielastic broadening vs the temperature. The dashed line represents the experimental resolution.

vector. The weak quasielastic wings observed at higher Q (see also Fig. 2) are still due to isotropic rotational motion with the same diffusion coefficient $D_r=4\times10^9\,\text{s}^{-1}$.

In fact, translational diffusion mobility is measurable only at $T\geqslant265\,\text{K}$. Figure 1(b) shows the evolution of the QENS signal versus the scattering vector at $T=270\,\text{K}$ and Fig. 2 displays its temperature behavior at a constant value of $Q=1.110\,\text{Å}^{-1}$. The broadening of the elastic peak at $T=265$ and 270 K corresponds to a translational diffusion coefficient D_t of $1.5(\pm0.5)\times10^{-5}\,\text{cm}^2\,\text{s}^{-1}$. The estimated proportion of liquid in the ice film is about 25% at $T=265\,\text{K}$, and 35% at $T=270\,\text{K}$. The rotational diffusion coefficient D_r increases with temperature since the best fit was obtained with $D_r=6.5(\pm1.0)\times10^9\,\text{s}^{-1}$ at $T=265\,\text{K}$ and $D_r=1.2(\pm0.2)\times10^{10}\,\text{s}^{-1}$ at $T=270\,\text{K}$.

It is worth comparing our coefficients to those obtained for the 3D liquid water.[4] A general point is that rotational diffusion coefficients found in our experiments are smaller (at least by one order of magnitude) than those measured in Ref. 4, whereas the translational diffusion coefficients are of the same order of magnitude at $T\geqslant265\,\text{K}$.

III. MOLECULAR DYNAMICS SIMULATION

A. Theoretical backgrounds

1. Interaction potential

The interaction potential for the adsorbate/substrate system has already been detailed elsewhere.[32] It is written as the sum of the water molecules/substrate interaction (V_{MS}) plus the lateral water–water interaction (V_{MM}). The water molecules and the MgO substrate are rigid. The potential V_{MS} is the sum of a dispersion–repulsion contribution represented by pairwise atom–atom Lennard-Jones interactions and of electrostatic terms. These latter terms describe the interaction between the electric field and field gradients created by the ionic substrate charges and the point dipoles and quadrupoles of the water molecules.[30] Note that the octupolar and higher order contributions as well as the polarization effects between the adsorbate and the substrate have been disregarded. They have a small influence on the first water layer, and are negligible for the upper layers of the film.[30,40] The electrostatic interactions between the film and the periodic substrate are expanded in the 2D reciprocal space of the substrate, in order to achieve a fast convergence of the calculations.

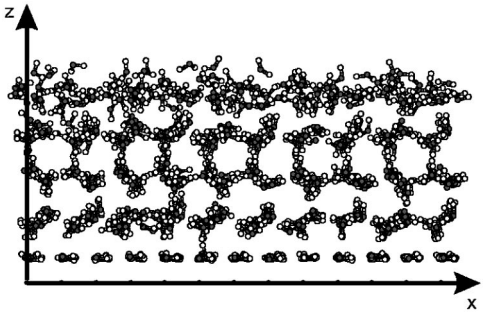

FIG. 3. Snapshot of the supported ice film at $T=220\,\text{K}$ showing the MgO surface ($z=0$), the flat ice monolayer, and the hexagonal ice bilayers.

The TIP4P model,[41] which accurately reproduces structure and dynamics of both ice and liquid water,[11] is used to describe the interaction V_{MM} between the water molecules. This model involves three charges located on the two protons and on a site slightly displaced with respect to the oxygen position along the C_{2v} molecular axis. A fourth site located on the oxygen characterizes the dispersion–repulsion interaction. For the lateral interactions, the sum is performed in the direct space, with a cutoff distance of 13.0 Å which gives almost the same results as the sum via the Ewald technique.[42]

2. Details of the simulation

The MD simulations are carried out by standard methods.[43] The ionic substrate is represented by six rigid layers of Mg and O ions, arranged according to the (001) geometry, which occupy the bottom of the simulation box. To be consistent with the experimental coverages, the simulation box contains five layers of moving water molecules adsorbed on MgO, thus forming a film of about 18 Å thick along **z** normal to the surface ($z=0$ is the MgO surface). The (x, y) size of the box ($x=35.9$ Å and $y=38.9$ Å, along the directions parallel to the MgO surface) obeys the requirement of commensurability between the five water layers and the substrate geometry. It corresponds to a repeated patch of size $12a_s\times13a_s$ (where $a_s=2.99$ Å is the substrate unit cell parameter). According to previous studies,[30,32] the innermost water layer has a flat geometry, whereas the four upper layers have the hexagonal structure of ice bilayers (Fig. 3). The monolayer contains 156 water molecules arranged in a flat geometry, whereas the upper layer's arrangement corre-

sponds to the replication along the x and y directions of an orthorhombic unit cell of proton ordered ice of dimensions $L_x = 8.97$ Å and $L_y = 7.77$ Å. This orthorhombic cell contains eight water molecules per bilayer,[44] and the simulation then implies a total of 796 moving water molecules for the five layers.

Beside, to quantify the influence of the substrate electric field on the dynamics of the water adlayers, simulations on pure ice are also performed for comparison. The MD box has the same (x, y) size as previously defined on MgO, i.e., by replicating the 8.97×7.77 Å^2 unit cell of ice, and contains six bilayers of moving water molecules placed on a slab consisting of two bilayers of fixed water molecules. This box contains a total of 1280 water molecules, 960 of which are moving molecules. The initial configuration of the water molecules[44] in the eight bilayers is defined according to the ice rules[45] and has no net charges or net dipoles.

The translational equations of motion are solved using the Verlet algorithm, and a predictor–corrector method based on the quaternion representation of the molecular orientations is used for the orientational equations of motion, with a time step of 2.2 fs. Long time runs are performed, involving 200 000 time steps (i.e., 440 ps) of equilibration and 50 000 additional time steps (110 ps) for collecting the data (production phase). The initial configuration for the water layers on MgO is obtained from an optimization procedure based on a previous study.[30] The initial velocities of each molecule are taken from a Boltzmann distribution corresponding to the desired temperature. The total energy of the system is held constant during the production runs by scaling the velocities every 20 steps. For simulation of such small size systems, the mean temperature is preserved quite well. According to the experiments, seven different temperatures are considered between 190 and 270 K.

3. Structural analysis and dynamics of the water layers

The translational ordering of the water molecules is studied at each temperature through the analysis of the distribution function $p(z)$, where z defines the distance of the water centers of mass to the MgO surface plane for the supported film or to the upper rigid ice layer for bulk ice. In a plane perpendicular to the $\mathbf{z}$ axis, we calculate three translational order parameters S_{Tm} $(m = 1,2,3)$ in order to characterize the displacements of the oxygen atoms from their ideal lattice positions when temperature is increased, as[5]

$$S_{Tm} = \frac{1}{N_L} \left\langle \left| \sum_j e^{i \mathbf{k_m} \cdot \mathbf{r}_j} \right| \right\rangle. \tag{5}$$

The sum over j accounts for the N_L molecules pertaining either to the four bilayers or to the outermost layer, only. The symbol $\langle \cdots \rangle$ means an average over the duration of a production run. $\mathbf{r}_j$ defines the position of the center of mass of the jth molecule in the absolute frame (x, y, z) and the three $\mathbf{k}_m$ are reciprocal lattice vectors associated to the perfect hexagonal ice structure in the (0001) basal plane, defined as

$$\mathbf{k}_1 = \frac{2\pi}{a_0}\left(-\frac{1}{\sqrt{3}}, 1, 0\right), \quad \mathbf{k}_2 = \frac{2\pi}{a_0}\left(\frac{2}{\sqrt{3}}, 0, 0\right), \quad \mathbf{k}_3 = \frac{2\pi}{a_0}\left(-\frac{1}{\sqrt{3}}, -1, 0\right), \tag{6}$$

where a_0 corresponds to the hexagonal unit cell parameter of bulk ice.

The orientational ordering of the water layers is analyzed through the calculation of rotational order parameter S_R defined as[5]

$$S_R = -6.779 \times \left[\frac{1}{N_L} \sum_j \left(e_{x_j}^4 + e_{y_j}^4 + e_{z_j}^4 \right) - 0.6 \right], \tag{7}$$

where the sum is over the N_L water molecules, and $(e_{x_j}, e_{y_j}, e_{z_j})$ are the components in the absolute frame of a unit vector along the molecular axis of the jth molecule. For the perfectly proton ordered ice crystal, S_{Tm} and S_R are normalized to 1, while they vanish for the liquid. Orientational ordering is also characterized by the distribution functions of the three Euler angles (θ, ϕ, and ψ) defining the orientations of the water molecules with respect to the absolute frame.

To characterize the translational mobility of the water molecules in the whole film or in its outermost layer, self-diffusion coefficients are calculated from the linear behavior at long times of the mean-square displacements of the molecular centers of mass,[46] as

$$D_t = \frac{1}{6} \lim_{t \to \infty} \frac{d}{dt} \langle |\mathbf{r}_j(t) - \mathbf{r}_j(0)|^2 \rangle. \tag{8}$$

Furthermore, power spectra of the molecular centers of mass velocity autocorrelation functions (VACFs) which give the frequencies associated with the translational vibrations of the molecules are calculated for the layers.

To assess the rotational mobility of the molecules, the time autocorrelation function $C_1(t)$ of the first Legendre polynomial P_1 is calculated as[46]

$$C_1(t) = \langle P_1[e_{z_j}(t) \cdot e_{z_j}(0)] \rangle. \tag{9}$$

This function is plotted in the logarithmic form since the orientational diffusion coefficient is associated with the limiting linear behavior of $0.5 \ln C_1(t)$ at times much longer than the angular velocity correlation time τ_ω[47] as

$$\lim_{t \gg \tau_\omega} 0.5 \ln C_1(t) = D_r \times t \equiv \frac{t}{2\tau_c}, \tag{10}$$

where τ_c defines the reorientational correlation times. The orientational diffusion coefficient D_r is then defined as $(2\tau_c)^{-1}$. The librations of the water molecules are characterized by the correlation time τ_ω obtained from the angular velocities autocorrelation function $\langle \omega_j(t) \omega_j(0) \rangle$ (AVACF). While τ_ω is related to the main librational features which appear in infrared and Raman spectra,[46] τ_c corresponds to the reorientation time of the water molecules, and largely determines the nuclear magnetic resonance relaxation time.[46]

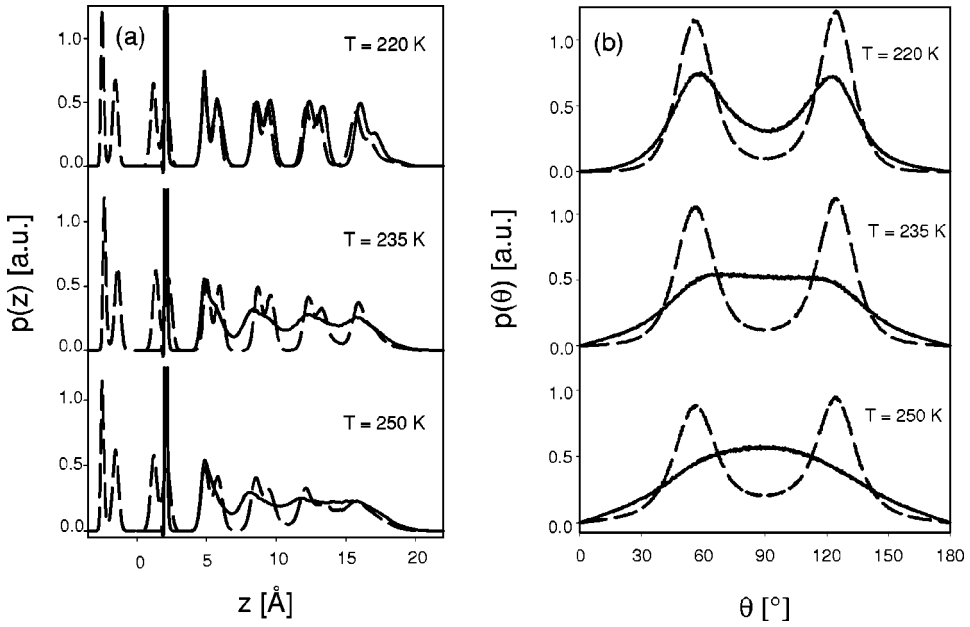

FIG. 4. (a) Distribution function $p(z)$ (in arbitrary unit) of the water centers of mass with respect to the distance z to the MgO(001) surface (note that the z origin for the bulk ice is taken at the position of the upper rigid water layer; see the text) and (b) polar angular distribution function $p(\theta)$ of the water dipole moment with respect to the z axis at different temperatures. Full curves correspond to the supported ice film and broken curves to bulk ice.

B. Results

1. Structure of the water film

The distribution function $p(z)$ for the H_2O/MgO system is shown in Fig. 4(a) at three temperatures. The single peak at 2.12 Å corresponds to the formation of the flat water monolayer above MgO,[30,32] and the other double peaks (full curve) at higher z values characterize the translational ordering of the water layers consistent with the hexagonal ice structure.[48] Up to 220 K, the translational ordering for the four upper water layers on MgO is very similar to that calculated for bulk ice, as indicated by the superimposition with the distribution function $p(z)$ (broken curve) for a slab of ice in Fig. 4(a). Let us note that the double peaks are less pronounced for the outermost layer of both bulk ice and supported film due to large amplitude motions of the molecules in the outermost layer, even at these low temperatures.[20] Note also the small shift of the peak maxima characterizing the outermost layers of the supported film which is the result of the substrate influence. At higher temperature, the two systems exhibit a different behavior. Indeed, the doublet structure for all the layers of the supported film disappears above 230 K, indicating melting of the bilayer structure of the water film, whereas it can still be observed for bulk ice up to 250 K, indicating that some translational order remains in $p(z)$ for this latter case, at least for the innermost water layers. In fact, for pure ice, the doublet structure disappears above 270 K only.

A similar behavior is obtained for the angular distribution functions. In Fig. 4(b), two well-defined peaks occur around 55° and 125° in the distribution function $p(\theta)$ for both the supported film and bulk ice at 220 K (note that we have removed the contribution of the flat monolayer in the distribution function corresponding to the supported film). By contrast, at $T > 235$ K, the curve $p(\theta)$ for the supported film exhibits a broad distribution of angles as it should be the case for a liquid-like layer, whereas two peaks remain clearly for pure ice, up to 250 K.

The translational S_T and orientational S_R order parameters for the whole supported film (except for the monolayer) and for its outermost layer are given in Fig. 5 as functions of temperature. Note that S_T is given as an average of the three symmetry-related S_{Tm}. Figure 5(a) shows that some parallel translational order remains up to 230 K for the supported film (full curve) since the translational order parameter is larger than 0.3, while it decreases abruptly around 230 K and vanishes above. The same conclusion is obtained for the surface layer [Fig. 5(b)] which exhibits, however, a much larger disorder than the film even at the lowest temperatures ($T \leqslant 200$ K). For comparison, the S_T parameter is also given for bulk ice (broken curve). Above 220 K, the surface layers of both supported and pure ice behave similarly. On the contrary, the innermost layers are much more structured in pure ice than in the supported film, as exhibited by the larger

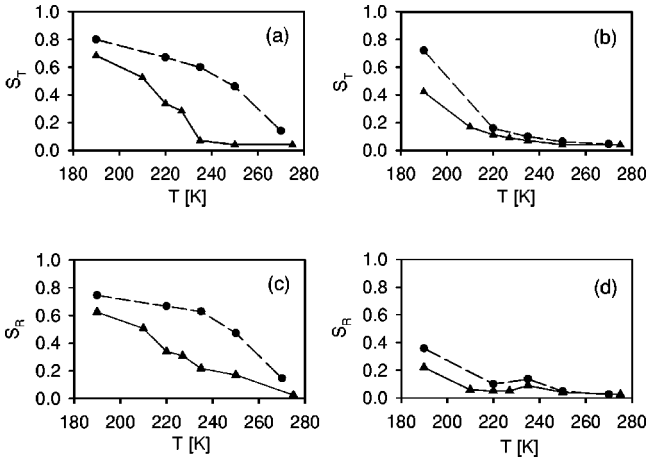

FIG. 5. Translational order parameters S_T vs temperature for (a) the whole ice film (four supported or bulk bilayers) and (b) the outermost bilayer only. Orientational order parameters S_R vs temperature for (c) the whole ice film (four supported or bulk bilayers) and (d) the outermost bilayer only. Full curves correspond to the supported film and broken curves to bulk ice.

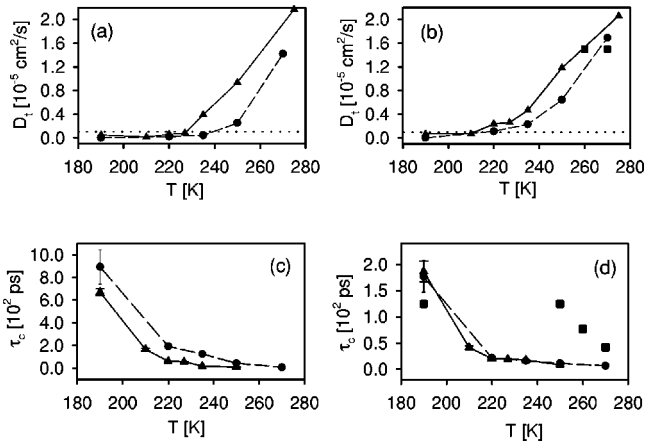

FIG. 6. Translational diffusion coefficient D_t (10^{-5} cm^2 s^{-1}) vs temperature for (a) the whole ice film and (b) the outermost bilayer. Orientational correlation time $\tau_c=(2D_r)^{-1}$ in ps vs temperature for (c) the whole ice film and (d) the outermost bilayer. Full curves correspond to the supported film and broken curves to bulk ice. The experimental data are also given (full squares) with the corresponding experimental detection limit (dotted line) for D_t.

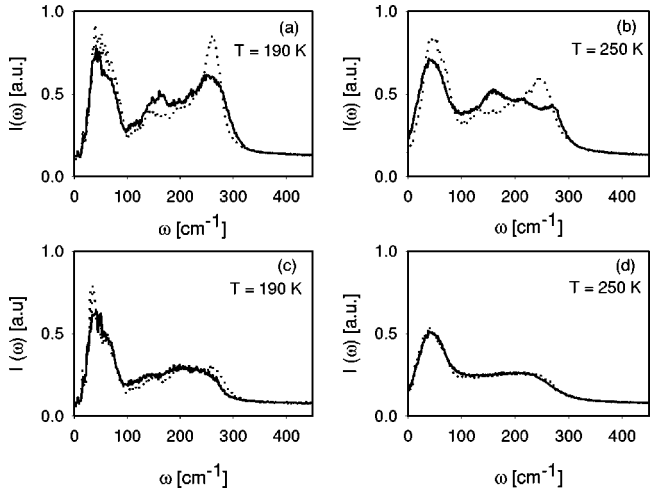

FIG. 7. Power spectrum (in arbitrary unit) of the linear velocity autocorrelation function for the water molecules at two temperatures: (a) and (b) for the whole film, and (c) and (d) for the outermost bilayer. Full curves correspond to the supported film phonon density of states and dotted curves to bulk ice phonons.

values of the translational order parameters in the former case up to 260 K.

Similar conclusions can be drawn from the analysis of the rotational order parameters [Figs. 5(c) and 5(d)] which shows that the rotational disorder appears above 200 K for the outermost layer of the ice film, whereas some order remains in the rest of the film up to 230 K. Again, the curves S_R for the surface layer of both the supported film and bulk ice behave similarly, whereas the innermost water layers are much more orientationally disordered on MgO than in pure ice. It may be seen that the sudden decrease observed for S_T for the supported film around 230 K is not so abrupt for S_R.

2. Dynamics of the film

Figure 6(a) displays the calculated translational diffusion coefficient $D_t(T)$ [Eq. (8)] for the supported ice film together with bulk ice. Although the curves are only guides for the eye, we see that the film mobility is nearly constant and less than 10^{-6} cm^2 s^{-1} when the temperature is lower than 230 K. At higher T, the mobility increases rapidly to reach 10^{-5} cm^2 s^{-1} at 250 K and 2×10^{-5} cm^2 s^{-1} at 270 K. This latter value is close to the liquid value at 270 K.[4]

The diffusion coefficient for the outermost layer of the film is drawn in Fig. 6(b). The behavior is rather similar to that of the whole film, except for an overall shift toward the low temperatures, indicating an enhanced mobility of this layer. At 220 K, the diffusion coefficient of the outermost layer is 5 times larger than for the whole film, increasing from 5×10^{-7} to 2.5×10^{-6} cm^2 s^{-1}. At 250 K, D_t is equal to 10^{-5} cm^2 s^{-1} for the whole film and to 1.2×10^{-5} cm^2 s^{-1} for the outermost layer. The same calculations carried out for bulk ice show that the translational mobility is smaller than for the supported film, since at 250 K the D_t value is 4 times smaller for the whole film, and 2 times smaller for the outermost layer.

Similar comparisons are done to analyze the orientational mobility of the film as a function of temperature, through the behavior of τ_c, as discussed in Sec. III. $\tau_c(T)$ is drawn in Fig. 6(c) for the whole film and in Fig. 6(d) for its outermost layer. In Fig. 6(c), the orientational correlation time τ_c strongly decreases from 670 ps at 190 K to 60 ps at 220 K for the whole film and then varies much more slowly to reach a value less than 10 ps at 250 K. The same curve drawn for bulk ice exhibits a shift, indicating a smaller orientational mobility in this latter case, already present for the lowest temperature (190 K). At 220 K, the supported film appears to be 4 times more mobile than bulk ice. The calculated orientational mobilities of the outermost layer of both bulk ice and supported film behave similarly, with a strong decrease when T increases up to 210–220 K and then with a nearly constant slope of the curve $\tau_c(T)$ when T grows to 270 K. These outermost layers are extremely mobile when compared to the whole film, even at 190 K, and the calculated value of τ_c decreases from 20 ps at 220 K to a few ps above 250 K. For comparison, the measured value of τ_c for the liquid is 2 ps at 300 K.[46]

3. Power spectrum

At 190 K, the calculated power spectrum $I(\omega)$ of the VACF $\langle \mathbf{v}(0)\mathbf{v}(t)\rangle$ for the supported film exhibits a peak at about 45 cm^{-1} and two ill-resolved broad peaks around 155 and 255 cm^{-1} [Fig. 7(a)]. Except for the peak at 155 cm^{-1}, which is independent of the temperature, and which can be assigned to the flat monolayer, the other structures are similar to those calculated for bulk ice, though they are less peaked. The lowest frequency peak was assigned to O···O···O bending and the highest frequency peak to O···O stretch.[49] At 250 K, the peak at 255 cm^{-1} disappears for the supported film while it is still present for bulk ice [Fig. 7(b)].

The corresponding spectra for the outermost layer [Figs. 7(c) and 7(d)] display the single peak already mentioned around 45 cm^{-1}, with a single broad high-frequency shoulder spreading out up to 270 cm^{-1}. The shapes of these spectra for the supported film and bulk ice are nearly superim-

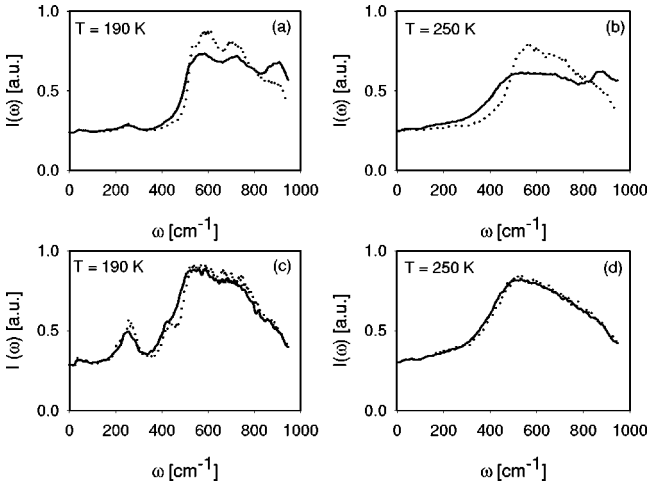

FIG. 8. Power spectrum of the angular velocity autocorrelation function for the water molecules at two temperatures: (a) and (b) for the whole film, and (c) and (d) for the outermost bilayer. Full curves correspond to the supported film phonon density of states and dotted curves to bulk ice phonons.

posed, indicating a very similar behavior of the outermost layer dynamics in the temperature range 190–270 K.

A comparison between Figs. 7(b) and 7(d) shows that the phonon spectrum of the supported film at 250 K looks like that of the outermost layer, when the signal characteristic of the monolayer is subtracted. Indeed, the higher frequency peak of supported ice phonons disappears and it is replaced by a broad structure characteristics of the liquid.[46] From these features, we see that the supported film at 250 K has a liquid-like behavior, whereas the corresponding phonon spectrum of bulk ice at 250 K still displays the signature of the solid.

The spectrum associated with the AVACF $\langle \omega(0)\omega(t)\rangle$ is given in Fig. 8. The spectra at 190 and 250 K for the outermost layers [Figs. 8(c) and 8(d)] are nearly superimposed, with a broad structure extending from 350 to 900 cm^{-1} and corresponding to librational motions,[49] and an additional peak around 250 cm^{-1} which disappears at higher temperature. By contrast, more pronounced differences shown in Figs. 8(a) and 8(b) occur when the whole film is considered. The main structure broadens with temperature in both cases (supported film and bulk ice), but the broadening is more significant for the supported film, leading to a structureless shape at 250 K. Note, however, the presence of the 250 cm^{-1} frequency peak at 190 K characteristic of ice which disappears completely at 250 K, indicating the transition toward a liquid.

Examining these features, we can consider that, from both translational and orientational points of view, a transition from solid to liquid-like phase occurs around 235 K for the whole supported film and above 250 K for bulk ice. Regarding the behavior of the outermost layer for both systems, it appears rather liquid-like, even at the lowest temperatures considered here.

IV. DISCUSSION

A. Comparison between MgO supported film and bulk ice

The present results obtained for the ice film supported by MgO(001) and for the same thickness of ice deposited on bulk ice lead to the conclusions that (i) the structural (translational+orientational) disorder is always larger for the supported film, and (ii) the translational and orientational dynamics of the film is more rapid, leading to a lower melting temperature. This is consistent with the idea that the support should influence the solid/liquid-like transition in an ice film. By contrast, the outermost water layers of both the film and bulk ice have the same structural and dynamical behavior, i.e., solid-like below 220 K and close to the liquid at higher temperatures. This behavior is corroborated by the shapes of the phonon and libron density of states, which are very similar for the outermost layer of the supported film and bulk ice.

Previous experimental and theoretical studies[5,11] have confirmed that surface melting occurs on ice crystals, but even recent experiments[50] conducted on the molecular-scale structures of ice surfaces have not elucidated the solid/liquid transition mechanism due to the difficulty of direct observation. Therefore, data on the bulk ice surface melting are mainly issued from simulations. More particularly, Nada and Furukawa[8,11] have studied the melting of ice surface using the TIP4P model to describe water–water interactions. From a structural analysis of the ice surface, they mentioned the appearance of a disruption of hydrogen bonding network in the outermost layer around 215 K which they attribute to surface melting. Then, they determined the thickness of the resulting quasiliquid layer at the ice surface as a function of temperature by carrying out molecular dynamics simulations from 170 to 250 K, and they analyzed the layer-by-layer melting. It was thus shown that the surface layer is disordered at 225 K while the layers underneath keep their solid arrangement, and that the melting of the second and third layers occurs at 250 K.

Our results on bulk ice agree well those of Nada and Furukawa[8,11] and compare reasonably with results of previous simulations[5–13] also performed on bulk ice but based on different working hypotheses, including the choice of the interaction potential, the size of the simulation box, and the initial structure of ice. In the present paper, we have considered a proton ordered structure to describe the initial structure of bulk and supported ice. A technical reason motivated such a choice to limit the size of the ice unit cell and to achieve commensurability with the MgO support. However, we are aware that proton disordered phases could be more probable at finite temperature. Simulations on proton disordered phases are possible over a very restricted sampling of such phases,[5,12] and it has been shown that the calculations leading to the main characteristics of bulk ice were not significantly different using either proton ordered or disordered ice as initial system. Regarding the simulation box and, in a concomitant way, the cutoff distance for the intermolecular potential, it is known that too restrictive simulation boundary conditions can have a dramatic effect on dynamical proper-

ties and a much less sensitive influence on the structural properties of water.[16] The present size of the simulation box (more than 35 Å) and the corresponding cutoff value of 13 Å for the long-range water–water potential including a polynomial damping function seem to be reasonable for describing conveniently long-range correlations of the translational and orientational coordinates of water molecules. Such large values probably make the need for technical refinements less mandatory, mainly Ewald summation or reaction field boundary conditions which are time consuming.[16]

Examining previous data on bulk ice and our results, it is clear that the choice of TIP4P potential is responsible in general for a shift of the melting temperature when compared to the experimental data. Many simple semiempirical potentials have been used and improved in the last ten years.[17,41,51–56] Unfortunately, none of them can account in an extensive and accurate way for the properties of both liquid and ice water. The more extensively used forms were probably the SPC model for the liquid[16] and the TIP4P potential which seemed more adequate for ice.[8,10] With this latter potential, a rescaling coefficient for the temperature leading to surface melting of bulk ice seems to be needed, corresponding to a high temperature shift of 20–30 K. Our results for bulk ice agree with this feature, and we can expect that the same rescaling factor should be applied to the supported ice film. This assumption would improve in a significant way the agreement with the neutron scattering experiments.

B. Comparison between experimental data and simulation results

The neutron diffraction spectrum of D_2O on MgO(001)[33] displays at 190 K a superimposition of a broad peak characteristic of the monolayer and of the (100), (002), (101), and (102) peaks associated with the hexagonal ice structure of the upper layers. The (002) peak is however broadened when compared to bulk ice, indicating rather the formation of thin film than of bulk ice. The ice signature disappears at about 273 K, and it is replaced by a broad structure which characterizes the presence of a liquid film, whereas the monolayer signal remains present. It is worthwhile to recall that the melting temperature of D_2O is 276.82 K. In the simulation, the translational and orientational order parameters decrease strongly when temperature increases and the structural order of the water molecules is entirely lost in the supported film for $T > 230-240$ K. Comparison with experiments thus shows a shift of about 30 K for the transition temperature from an ordered to a disordered structure of the supported film.

From the quasielastic neutron scattering spectra we have determined, via diffusion models, the translational and orientational mobilities. No translational mobility (less than the detection limit $D_t^l \sim 10^{-6}\,\mathrm{cm^2\,s^{-1}}$) has been detected below 250 K. Therefore, the two measurements reported in Fig. 6 correspond to mobilities around $1.5\times10^{-5}\,\mathrm{cm^2\,s^{-1}}$ for $T = 265$ and 270 K. At these temperatures, the calculated values agree quite well with the measurements. However, the simulation results indicate that a translational mobility larger than D_t^l should be detected above 230 K. Regarding the orientational mobility, experiments show that τ_c remains nearly constant when T increases from 190 to 250 K, and abruptly decreases from 125 ps at 250 K to 40 ps at 270 K. In the simulations, the values of τ_c at 190 and 270 K are close to the experimental data and the slope of the curve $\tau_c(T)$ is similar to the experimental one. However, in order to reproduce the experimental temperature variation of τ_c a shift of about 40 K is required.

A comparison between the present experiments and calculations shows a temperature shift within the range 30–40 K regarding the transition from solid to liquid behavior of the supported ice film. This range depends on the physical quantity under consideration (translation/orientation or structure/dynamical factors). An accurate experimental value of the surface melting transition is not available yet. Nevertheless, our QENS measurements indicates that a mobile layer showing a translational diffusion coefficient close to that of liquid water appears between 250 and 265 K. Hence, one may reasonably infer that the surface melting transition occurs within this temperature range. A large uncertainty also exists regarding the estimate of the transition temperature from simulation results. Indeed, the curves connected to both order parameters and diffusion coefficients are only guides for the eye and they do not exhibit abrupt breakings in their slope as would be the case for a first-order transition.

Recent neutron diffraction experiments indicate that an ordered ice Ih film still exists at $T = 265$ K.[57] These results, combined with those of the present QENS experiments, show that at this temperature the liquid fraction coexists with an ice Ih film. Our molecular dynamics simulations indicate clearly that this mobile phase concerns the outermost surface layers of the ice thin film.

In Sec. II A, we pointed out that our present QENS experiments are performed with an equivalent 5 BL ice film on MgO(001). In fact, we cannot rule out the possible formation of thicker ice crystallites due to substrate inhomogeneities or condensation on the cell walls. In that case, our experimental data would be characteristic of a situation somewhat intermediate between results of simulations performed on bulk ice and on supported ice film. However, this consideration would not significantly change our main conclusions on the comparison between experiments and simulations.

C. Comparison with other data

The calculated power spectra connected to phonons and librons of bulk ice compare fairly with previous simulation results in the literature using the same TIP4P potential. They are also in fair agreement with phonon data issued from other potential models and inelastic neutron scattering experiments. The experimental peaks, observed around 75, 150, and 225 $\mathrm{cm^{-1}}$ at very low temperature,[58] correspond to hexagonal ice signals which are calculated here around 50, 150, and 255 $\mathrm{cm^{-1}}$ in Fig. 7(a), at 190 K. The same inelastic spectrum observed at 260 K[59] still exhibits the peaks around 75 and 150 $\mathrm{cm^{-1}}$, but the higher frequency peak is replaced by a broad structure spreading out up to 300 $\mathrm{cm^{-1}}$. This latter profile is close to the spectrum calculated in this paper at 250 K for the supported film. These experimental data thus

corroborate the results of simulation that below 230 K the supported water layers are solid, while they are rather liquid-like at higher temperature.

As mentioned in the Introduction, the number of studies on supported films of ice within the temperature range 200–300 K is very limited and very recent. Ewing *et al.*[60] used infrared spectroscopy to show that water adsorbs onto NaCl(001) forming a liquid-like film between 245 and 315 K, with the formation of saturated salt solution. Water film deposition on mica surface was studied by Salmeron *et al.*[61,62] using sum frequency generation (SFG) and scanning polarization force microscopy. The structure of the water bilayer closer to the mica surface at ambient temperature looks like the ice structure, though distorted when compared to the original Ih geometry. Below 273 K, ice films a few bilayers thick are formed, which are covered by liquid-like water. While liquid water does not wet ice at 240 K, a transformation toward wetting liquid is observed near 255 K. However, up to 273 K the orientational ordering observed in the innermost bilayer continues into the subsequent bilayers. Other recent atomic force microscopy studies of ice surface between 250 ad 272 K have investigated the thickness of the liquid-like layer on ice by correlating the liquid/solid transition with an increase of the adhesion force and viscosity.[63–65] Liquid phase thicknesses of 10 to 100 Å were measured depending on the tip stiffness.

Quartz/water and quartz/ice interfaces were studied by Shen *et al.* using sum frequency generation spectroscopy.[66] They showed that the structure at the vapor/water interface is ice-like, though less ordered than bulk ice. This conclusion seems to apply to all water interfaces with, however, different degrees of ordering according to the support properties and physical conditions. As a result, they do not find a quasiliquid layer at the quartz/ice interface, i.e., no surface melting.

Our conclusions for the MgO supported film are different. From both experiments and calculations, ice melting occurs well below 270 K on MgO(001). By no means does the support tend to strengthen the film network; on the contrary, it favors translational and orientational disorder. This different behavior can be due to different experimental conditions (preparation of the sample) and/or to the probe (neutrons do not probe the same observables as SFG). It can also be due to the support properties: Ice ordering on MgO proceeds in such a way that a flat monolayer is formed first with no significant hydrogen bonding with MgO nor with the upper bilayers. By contrast, on Pt(111), mica, and quartz surfaces, strong H bonds are formed with the substrate which tend to keep ice geometry in the adsorbed water layers.

V. CONCLUSION

Combined neutron scattering experiments and molecular dynamics calculations have been presented to determine the melting temperature of a thin ice film (five layers) supported on the MgO(001) surface. From quasielastic neutron scattering experiments translational and orientational mobilities are detected at 265 K, whereas no significant translational mobility occurs below 250 K. Molecular dynamics calculations using the TIP4P potential model show a transition from the solid to a liquid-like phase on both supported ice film and bulk ice, though the absolute value of the melting temperature appears slightly underestimated with respect to experimental data. Using a rescaling factor of about 20–30 K, which is typical of the TIP4P model, as determined from a comparison with bulk ice simulations, it becomes possible to interpret quantitatively the behavior of a thin ice film supported by an ionic substrate over the temperature range 190–270 K and, especially, the surface melting transition.

ACKNOWLEDGMENTS

The authors kindly acknowledge the LLB for giving us access to the neutron facilities and R. Kahn for having accepted to be our local contact. They are also grateful to J. P. Coulomb, M. Bienfait, and J. M. Gay for fruitful discussions about the interpretation of the QENS spectra.

[1] S. Solomon, R. R. Garcia, F. S. Rowland, and D. J. Wuebbles, Nature (London) **321**, 755 (1986).
[2] M. J. Molina, R. Zhang, P. J. Wooldridge, J. R. McMahon, J. E. Kim, H. Y. Chang, and K. D. Beyer, Science **261**, 1418 (1993).
[3] J. S. Wettlauffer, J. G. Dash, and N. Untersteiner, *Ice Physics and the Natural Environment*, NATO ASI Series I, Vol. 56 (Springer, Berlin, 1999).
[4] S. H. Chen and J. Teixeira, Adv. Chem. Phys. **64**, 1 (1986).
[5] For a review, see for instance: G. J. Kroes, Surf. Sci. **275**, 365 (1992); Comments At. Mol. Phys. **34**, 259 (1999).
[6] O. A. Karim and A. D. J. Haymet, J. Chem. Phys. **89**, 6889 (1988).
[7] F. Sciortino and G. Corongiu, J. Chem. Phys. **98**, 5694 (1993).
[8] H. Nada and Y. Furukawa, J. Phys. Chem. B **101**, 6163 (1997).
[9] C. J. Burnham, J. C. Li, and M. Leslie, J. Phys. Chem. B **101**, 6192 (1997).
[10] M. J. Vlot, J. Huinink, and J. P. van der Eerden, J. Chem. Phys. **110**, 55 (1999).
[11] H. Nada and Y. Furukawa, Surf. Sci. **446**, 1 (2000).
[12] G. T. Gao, X. C. Zeng, and H. Tanaka, J. Chem. Phys. **112**, 8534 (2000).
[13] K. Bolton and J. B. C. Petterson, J. Phys. Chem. B **104**, 1590 (2000).
[14] D. Heisenberg and W. Kauzmann, *The Structure and Properties of Water* (Clarendon, Oxford, 1969).
[15] S. B. Zhu, S. Singh, and G. W. Robinson, Adv. Chem. Phys. **85**, 627 (1994).
[16] D. van der Spoel, P. J. van Maaren, and H. J. C. Berendsen, J. Chem. Phys. **108**, 10220 (1998).
[17] M. W. Mahoney and W. L. Jorgensen, J. Chem. Phys. **112**, 8910 (2000).
[18] M. Morgenstern, J. Müller, T. Michely, and G. Comsa, Z. Phys. Chem. (Munich) **198**, 43 (1997).
[19] A. Glebov, A. P. Graham, A. Menzel, and J. P. Toennies, J. Chem. Phys. **106**, 9382 (1997).
[20] N. Materer, U. Starke, A. Barbieri, M. A. van Hove, G. A. Somorjai, G. J. Kroes, and C. Minot, Surf. Sci. **381**, 190 (1997).
[21] D. E. Brown and S. M. George, J. Phys. Chem. **100**, 15460 (1996).
[22] F. E. Livingston, G. C. Whipple, and S. M. George, J. Chem. Phys. **108**, 2197 (1998).
[23] J. C. Zink, J. Reif, and E. Matthias, Phys. Rev. Lett. **24**, 3595 (1992).
[24] A. Lehmann, G. König, and K. H. Rieder, Phys. Rev. Lett. **73**, 3125 (1994).
[25] S. Fölsch and M. Henzler, Surf. Sci. **247**, 289 (1991).
[26] L. W. Bruch, A. Glebov, J. P. Toennies, and H. Weiss, J. Chem. Phys. **103**, 5109 (1995).
[27] J. Heidberg, B. Redlich, and D. Wetter, Ber. Bunsenges. Phys. Chem. **99**, 1333 (1995).
[28] D. Ferry, A. Glebov, V. Senz, J. Suzanne, J. P. Toennies, and H. Weiss, J. Chem. Phys. **105**, 1697 (1996).
[29] D. Ferry, A. Glebov, V. Senz, J. Suzanne, J. P. Toennies, and H. Weiss, Surf. Sci. **377–379**, 634 (1997).
[30] D. Ferry, S. Picaud, P. N. M. Hoang, C. Girardet, L. Giordano, B. Demirdjian, and J. Suzanne, Surf. Sci. **409**, 101 (1998).
[31] M. I. McCarthy, G. K. Schenter, C. A. Scamehorn, and J. B. Nicholas, J. Phys. Chem. **100**, 16989 (1996).

[32] A. Marmier, P. N. M. Hoang, S. Picaud, C. Girardet, and R. M. Lynden-Bell, J. Chem. Phys. **109**, 3245 (1998).
[33] B. Demirdjian, J. Suzanne, D. Ferry, J. P. Coulomb, and L. Giordano, Surf. Sci. **462**, L581 (2000).
[34] J. P. Coulomb and O. E. Vilches, J. Phys. **45**, 1381 (1984).
[35] J. P. Coulomb, T. S. Sullivan, and O. E. Vilches, Phys. Rev. B **30**, 4753 (1985).
[36] J. P. Coulomb, K. Madih, B. Croset, and H. J. Lauter, Phys. Rev. Lett. **54**, 1536 (1985).
[37] M. Bée, *Quasielastic Neutron Scattering* (Hilger, Bristol, 1988).
[38] A. J. Dianoux, F. Volino, and H. Hervet, Mol. Phys. **30**, 1101 (1970).
[39] J. Teixeira, M. C. Bellissent-Funel, S. H. Chen, and A. J. Dianoux, J. Phys. C **45**, 7 (1984).
[40] C. Toubin, S. Picaud, and C. Girardet, Chem. Phys. **244**, 227 (1999).
[41] W. L. Jorgensen, J. Chandrasekhar, J. F. Madura, R. W. Impey, and M. L. Klein, J. Chem. Phys. **79**, 926 (1983).
[42] R. S. Taylor, L. X. Dang, and B. C. Garret, J. Phys. Chem. **100**, 11720 (1996).
[43] M. P. Allen and D. J. Tildesley, *Computer Simulation of Liquids* (Clarendon, Oxford, 1987).
[44] V. Buch, private communication (1999).
[45] J. D. Bernal and R. H. Fowler, J. Chem. Phys. **1**, 515 (1933).
[46] R. W. Impey, P. A. Madden, and I. R. McDonald, Mol. Phys. **46**, 513 (1982).
[47] R. M. Lynden-Bell and I. R. McDonald, Mol. Phys. **43**, 1429 (1981).
[48] C. Toubin, P. N. M. Hoang, S. Picaud, C. Girardet, and R. M. Lynden-Bell, Surf. Rev. Lett. **6**, 1265 (1999).
[49] M. G. Sceats and S. A. Rice, J. Chem. Phys. **72**, 3236 (1980).
[50] H. Dosch, A. Lied, and J. H. Bilgram, Surf. Sci. **327**, 145 (1995); **366**, 43 (1996).
[51] H. J. C. Berendsen, J. P. M. Postma, W. F. von Gunsteren, and J. Hermans, in *Intermolecular Forces*, edited by B. Pullman (Reidel, Dordrecht, Holland, 1981), p. 331.
[52] O. Matsuoka, E. Clementi, and M. Yoshimine, J. Chem. Phys. **64**, 1351 (1976).
[53] N. Kumagai, K. Kawamura, and T. Yakowawa, Mol. Simul. **12**, 177 (1994).
[54] M. Sprik and M. L. Klein, J. Chem. Phys. **89**, 7556 (1988).
[55] C. Millot, J. C. Soetens, M. T. C. Martins Costa, M. P. Hodges, and A. J. Stone, J. Phys. Chem. A **102**, 754 (1998).
[56] T. M. Nymand and P. Linse, J. Chem. Phys. **112**, 6386 (2000).
[57] D. Ferry, B. Demirdjian, and J. Suzanne, unpublished results.
[58] J. C. Li, J. Chem. Phys. **105**, 6733 (1996).
[59] H. J. Prask, S. F. Trevino, J. D. Gault, and K. W. Kogan, J. Chem. Phys. **56**, 3217 (1972).
[60] M. Foster and G. E. Ewing, Surf. Sci. **427–428**, 102 (1999).
[61] M. Salmeron and H. Bluhm, Surf. Rev. Lett. **6**, 1275 (1999).
[62] H. Bluhm, T. Inoue, and M. Salmeron, Surf. Sci. **462**, L599 (2000).
[63] A. Döppenschmidt, M. Kappl, and H. J. Butt, J. Phys. Chem. B **102**, 7813 (1998).
[64] A. Döppenschmidt and H. J. Butt, Langmuir **16**, 6709 (2000).
[65] B. Pittenger, S. C. Fain, M. J. Cochran, J. M. K. Donev, B. E. Robertson, A. L. Szuchmacher, and R. M. Overney (unpublished).
[66] Y. R. Shen, Solid State Commun. **108**, 399 (1998), and references therein.